Journal of Materials Chemistry A

Accepted Manuscript

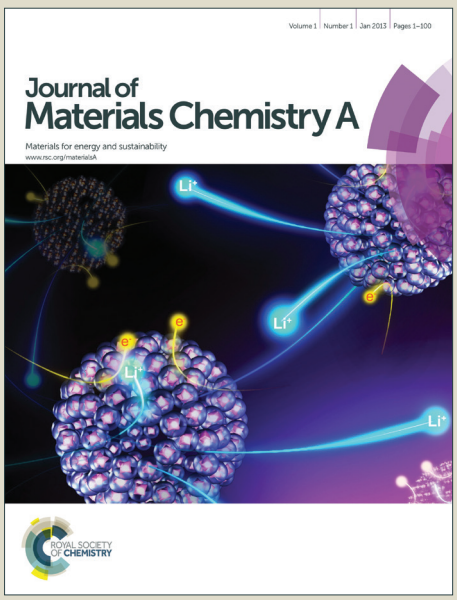

ROYAL SOCIETY OF CHEMISTRY

www.rsc.org/materialsA

Understanding the behavior of Li-oxygen cells containing LiI

Won-Jin Kwak[§], Daniel Hirshberg[†], Daniel Sharon[†], Hyeon-Ji Shin[§], Michal Afri[†], Jin-Bum Park[§], Arnd Garsuch[‡],Frederick Francois Chesneau[‡] , Aryeh A. Frimer[†], Doron Aurbach*[†] and Yang-Kook Sun*[§]

[§]Department of Energy Engineering, Hanyang University, Seoul, 133-791, South Korea.

[†]Department of Chemistry, Bar Ilan University, Ramat-Gan, 52900, Israel

[‡]BASF SE, GCI/E - M311, Ludwigshafen, 67056, Germany

*E-Mail addresses of corresponding authors: yksun@hanyang.ac.kr and aurbach@mail.biu.ac.il

Abstract

Mankind has been in a unending search for efficient sources of energy. The coupling of lithium and oxygen in aprotic solvents would seem to be a most promising electrochemical direction. Indeed, if successful, this system could compete with technologies such as the internal combustion engine and provide an energy density that would accommodate electric vehicle demands. All this promise has not yet reached fruition because of a plethora of practical barriers and challenges. These include solvent and electrodes stability, pronounced overvoltage for oxygen evolution reactions, limited cycle life and rate capability. One of the approaches suggested to facilitate the oxygen evolution reactions and improve rate capability is the use of red-ox mediators such as iodine for a fast oxidation of lithium peroxide. In this paper we have examined LiI as an electrolyte and additive in Li oxygen cells with ethereal electrolyte solutions. At high concentrations of LiI, the presence of the salt promotes a side reaction that forms LiOH as a major product. In turn, the presence of oxygen facilitates the reduction of I_3^- to $3I^-$ in these systems. At very low concentration of LiI, oxygen is reduced to Li_2O_2. The iodine formed in the anodic reaction serves as a red-ox mediator for Li_2O_2 oxidation.

Keywords: Electrochemistry, Li-oxygen batteries, Oxygen reduction, I_3^-/I^- red-ox couple

Table of Contents Graphic

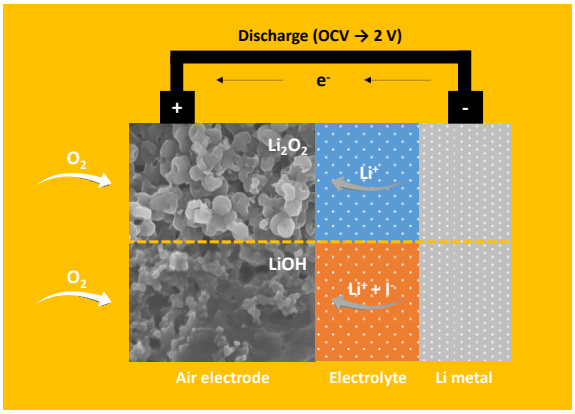

This work deals with core issues of Li-oxygen battery systems; intrinsic stability of poly-ether electrolyte solutions and the role of important red-ox mediators such as LiI/I_2.

Introduction

Ever since the industrial revolution, mankind has been in a frenzied search for more plentiful and efficient sources of energy. Cells twinning oxygen and lithium generates high hopes among electrochemists because of the many theoretical advantages of the Li/O_2 couple. These include: high specific energy, the simplicity of the preparation and operation of such electrochemical cells, and the substantial commercial opportunities. Indeed, the spiraling up of activity in this field over the past decade is testified to by the ever-increasing rate of new publications. The significant progress in the study of possible Li-O_2 battery systems has also prompted particular interest from the automotive and chemical industries.

Nevertheless, the study of Li-O_2 electrochemistry in aprotic solvents has been fraught with significant practical obstacles. One of the major challenges is the stability of the various Li-O_2 cell components to the presence of reduced oxygen species. In the early experiments on Li-O_2 cells this was largely neglected. The focus of exploration in the early works was the possibility of using molecular oxygen as an infinitely available active cathode material. These systems generally consisted of solid-state polymer electrolytes,[1] with liquid alkyl carbonates

electrolytes based cells used because of their wide application in Li-ion batteries technolgy.[2] A second wave of papers increasingly emphasized the discharge capacity by changing various parameters like oxygen solubility[3,4], cathode structure.[5,6] and different aspects in cell assembly.[7] In addition, there were many studies whose goal was to improve the low current densities and high over-potentials applied during cycling, by introducing catalysts into the cathode matrix.[8,9] Through all this early work, reversibility was never really checked; lithium-oxygen cells were commonly assumed to be "secondary batteries." The truth is, however, that these systems failed to achieve proper cyclability. This fault was compounded by the absence of analytical studies on the mechanism of the oxygen reduction reactions (ORR) and the corresponding oxygen evolution reactions (OER).

In the past five years, there have been a plethora of analytical techniques applied to the Li-O_2 system. *In situ* and *ex situ* methods like, XPS[10], AFM[11,12], Raman[13], FTIR[14], and DEMS[15,16] have helped to unravel the complex mechanisms of the Li-O_2 cell reactions. Recent work has revealed that, during ORR, in addition to the initial formation of lithium superoxide (LiO_2), assorted side products are generated – in particular, lithium peroxide (Li_2O_2) and lithium oxide (Li_2O) formed as outlined in Scheme 1.

1) $Li^+ + O_2 + e^- \rightleftharpoons LiO_2$

2) $2LiO_2 \rightleftharpoons Li_2O_2 + O_2$

3) $LiO_2 + Li^+ + e^- \rightleftharpoons Li_2O_2$

4) $2Li^+ + 2e^- + O_2 \rightleftharpoons Li_2O_2$

5) $Li_2O_2 + 2Li^+ + 2e^- \rightleftharpoons 2Li_2O$

Scheme 1. Main redox reactions related to O_2 reduction in Li-O_2 cells.

It should not be overlooked that the nucleophilicity and basicity of these reduced oxygen species [O_2^-, O_2^{-2} and O^{-2}] has been explored over the past few decades as part of the extensive studies on active oxygen chemistry in organic and aqueous solutions.[17,18] Of particular interest and concern is the reactivity of the various oxygen species toward the electrolyte solution and the carbon cathode. The exact influence of side reactions on cell performance is still under study and debate, though their presence is now indisputable.

An important development that refocused much attention on Li-oxygen batteries is the use of electro-catalysts. These were used to facilitate oxygen reduction and even more importantly, the oxidation of the Li_2O_2 precipitate, which is the major product of oxygen reduction in polar-aprotic systems.[19–22] Of major interest are reports that red-ox mediators in solution can be easily electrochemically oxidized and can then transfer electrons to Li_2O_2. The latter step considerably reduces the high over-voltage required to oxidize solid Li_2O_2.[23] One of the red-ox mediators recently studied in Li-oxygen cells was iodine.[24] Iodine and its reduced forms I_3^- and I^- (with Li^+ as the counter ion) are soluble in polar aprotic solvents. The electrochemistry of the I_3^-/I^- the I_2/I_3^- red-ox couples was studied two decades ago in both aqueous and non-aqueous solutions.[25] Considering that upon oxidation iodide forms iodine that in turn catalyzes the oxidation of Li-peroxide, the development of Li-oxygen cells with LiI as additive would, at first blush, look quite promising.

In the present work, the role of LiI in Li-oxygen cells employing polyether based electrolyte solutions was thoroughly explored. The present study further emphasizes how important possible side reactions are as a major limiting factor to the practical development of rechargeable Li-oxygen batteries. Understanding detrimental side reactions which occur in Li-oxygen systems is mandatory for advancing their R&D, which makes the present study very important for the field.

Experimental Section.

Materials: High purity di-glyme, tri-glyme and tetra-glyme (tetraethylene glycol dimethylether - TEGDME) polyethers were obtained from Sigma Aldrich and utilized as the solvents of the electrolyte solutions. $LiSO_3CF_3$ (Li-triflate, abbreviated here as LiTF from Sigma-Aldrich), $LiN(SO_2CF3)_2$ (LiTFSI , from Sigma Aldrich) and anhydrous LiI (Sigma Aldrich) where used as electrolytes. I_2 (Sigma Aldrich) was used as an additive. Li foil (Chemetall Foote Corporation, USA) was used for counter and reference electrodes. Fors oxygen reduction cathodes we used a carbonaceous gas diffusion layer (SIGRACET®GDL, SGL, 35BC) and activated carbon (TIMCAL, Super P®).

Preparation of Li−O_2 cells: We used several type of cells. For galvanostatic experiments coin type cells were prepared (from Wellcos parts) under argon atmosphere . In the reference cells, the caps of the cells formed hermetic seals under a pure Ar gas atmosphere).For experiments under oxygen, many holes were drilled into the caps allowing a free exposure of the cathode to oxygen (from the back side). For voltammetric studies, the same three electrodes cells used for EQCM measurements (see below) were employed. For *in-situ* EPR measurements, we used cells with a quartz capillary window which was assembled in the glove box; platinum served as both the working and counter electrodes, while 1M LiI in TEGDME functioned as the electrolyte solution. After assembly, the cell was flushed with pure oxygen and maintained at 1 atm oxygen.

For cathodes preparation, a mixture containing 80 wt% of Super P carbon and 20 wt% of polyvinylidene fluoride (PVDF, Alfa Aesar) was well mixed in a N-methyl-2-pyrrolidone (NMP) solvent and then coated onto a gas diffusion layer (SGL, 35BC) in a dry room. The carbon coated (~0.4 mg) electrodes were dried at 100 °C under vacuum for 12 h to remove the residual NMP solvent and cut to disks with 1.8 cm in diameter. Glass fiber separators

(GF/C, Whatman) were soaked with the electrolyte solution and lithium metal foils (thickness, 400 μm) were used as counter electrodes.

Electrochemical measurements: We produced gavanostatic and potentiostatic measurements with various solutions including 1M LiTF and LiTFSI in TEGDME and tri-glyme, 1M LiI in TEGDME (with and without I_2) and 1M LiTF/TEGDME solutions containing different amounts of LiI. Solvents were stored over 4Å molecular sieves in an Ar-filled glove box (final water content of <10 ppm, determined using a Mettler-Toledo Karl-Fischer titration). All cell assembliesy were carried out in argon-filled glove boxs (water and oxygen contents were less than 1 ppm). Before the test, cells were placed in an oxygen-filled chamber with a pressure slightly higher than 1 atm at room temperature and stabilized for 1 hr. The electrochemical measurements were carried out using computerized potentiostat-galvanostat VMP3 systems from Bio-Logic (France). Electrochemical quartz crystal microbalance (EQCM) measurements were carried out with a GAMRY (Warminster, USA) EQCM system. The working electrodes for these studies were platinum discs deposited on 5 MHz AT-cut quartz crystals (1.38 cm^2) (SRS, Sunnyvale, USA). A three ml electrochemical cell made of glass containing lithium counter and reference electrodes was used for the EQCM measurements. Before measurements, the electrolyte solutions were bubbled with high-purity oxygen for 30 min. All the measurements were carried out at room temperature (25 ^{0}C).

Characterizations: Before the analysis of electrodes after the discharge and charging processes, cycled cells were dismantled in Ar filled glove-box with less than 1 ppm H_2O and the cathodes were washed with anhydrous acetonitrile solvent and dried in vacuo for 1 hour. Then samples were transferred to the various analytical tools for characterization. Raman spectra were obtained using a Micro Raman HR800 spectrometer from Horiba Scientific Inc., with a near IR laser (in the range of 100 to 3100 cm^{-1}) at 632 nm. A field emission scanning

electron microscope (FE-SEM, JSM-6700F, JEOL) was employed to observe the morphology of the cathodes and the discharge products. The discharged and charged electrodes were protected from exposure to air during the transfer to the SEM ports with a portable evacuated transfer chamber. The presence of the ORR products on the carbon electrodes surfaces were analyzed using a AXS D8 Advance diffractometer (reflection θ-θ geometry, Cu Kα radiation (λ=1.54 Å), 0.6 mm slit, 40 mA, 40 kV) from Bruker, Inc. (Germany). The diffraction data were collected in the 2θ range from 20° to 80°, with a step size of 0.004°, at 2 s/step rate. The structural parameters and XRD patterns were carried out using the DIFFRAC SUITE-EVA software and Crystallography Open Database are part of the Bruker software package. The discharged electrodes were measured using a low background, air-tight specimen holder ring for small amounts of environmentally sensitive material (A100-B37 from Bruker, Inc., Germany). Sample reception is a 20mm diameter silicon wafer with high-index surface orientation. Electrode samples were also measured using a diffuse reflectance mode with an accessory from Pike Technologies. In-situ EPR measurements were performed using Elexsys 500-EPR system. The extraction of the EPR signal was accumulated while the cell was swept in a voltammetric mode at a rate of 0.1mV/s.

Results and discussion.

Reference electrochemical measurements - without LiI.

In order to analyze the role played by varying concentrations of iodide in the workings of lithium-air cells, it is important to establish first what exactly is transpiring prior to the addition of this redox additive. Figure 1 presents the typical response of Li-C electrochemical cells run under an oxygen atmosphere, where C refers to the carbon cathodes described in the experimental. Our TEGDME ethereal electrolyte solution in this system is 1M in LiTF or

LiTFSI and run while employing galvanostatic cycling with time limits of 1 and 10 hours (Figure 1a and 1b, respectively).

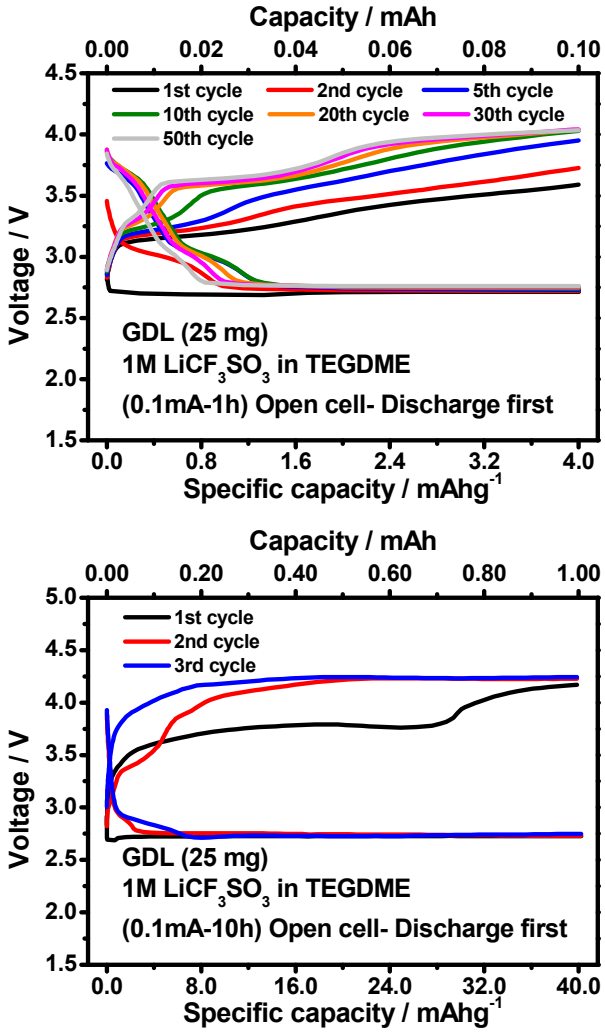

Figure 1. Galvanostatic cycling test response of Li–O_2 cells using 1 M $LiCF_3SO_3$ TEGDME at 0.1 mA current under time limit of (a) 1 h and (b) 10 h.

Within these time limits, the discharge is stopped prior to the end of the electrolytic processes. The latter would have normally terminated when oxygen reduction can no longer proceed due to blockage of the electrode by the precipitated reduction products. (Similar time limits of 1 h and/or 10 hours were also set for the cycling experiments depicted in Figures 2 and 3.) The

specific capacity values in the experiments presented herein are calculated per weight of the entire cathode material, including the gas diffusion layer, and they are not important for the purpose of the work and related discussions. Figure 1 shows periodic oxygen reduction (cathodic) and oxygen evolution (anodic) curves without catalysis.

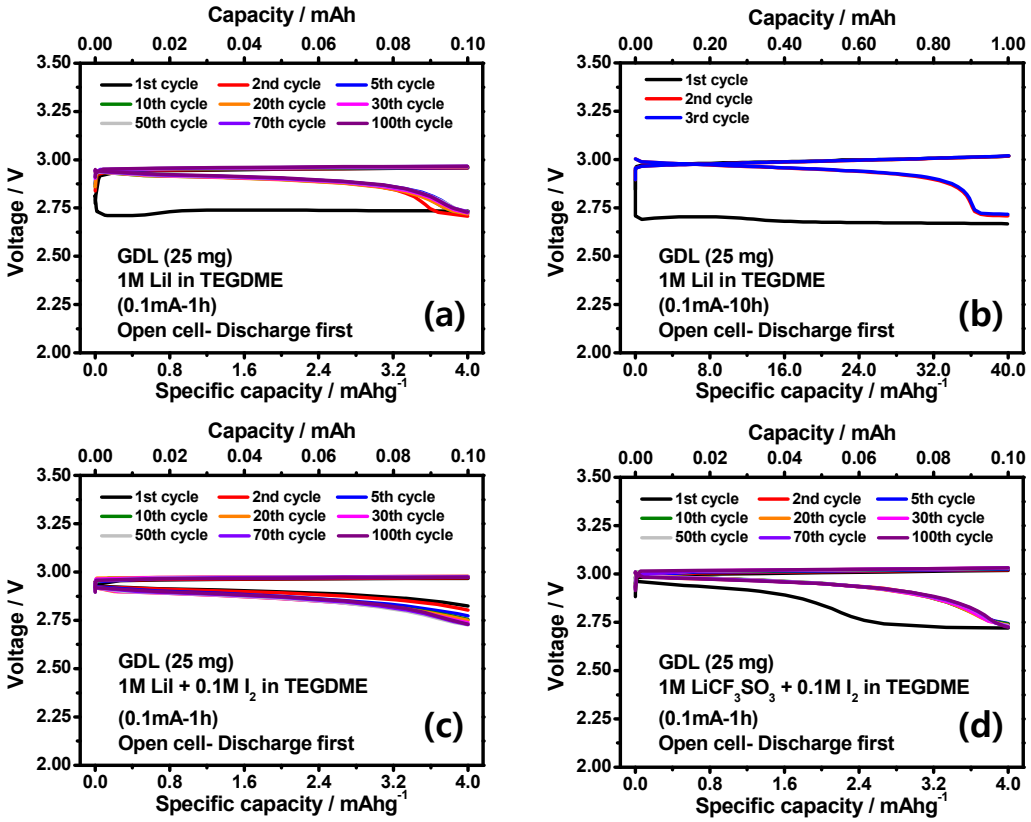

Figure 2. Galvanostatic cycling test response of Li–O_2 cells using different electrolytes with oxygen gas (open cell) at 0.1 mA current: (a) 1 M LiI in TEGDME under a time limit of 1 h; (b) 1 M LiI in TEGDME under time limit of 10 h; (c) 1 M LiI + 0.1 M I_2 in TEGDME; and (d) 1 M $LiCF_3SO_3$ + 0.1 M I_2 in TEGDME under a time limit of 1 h.

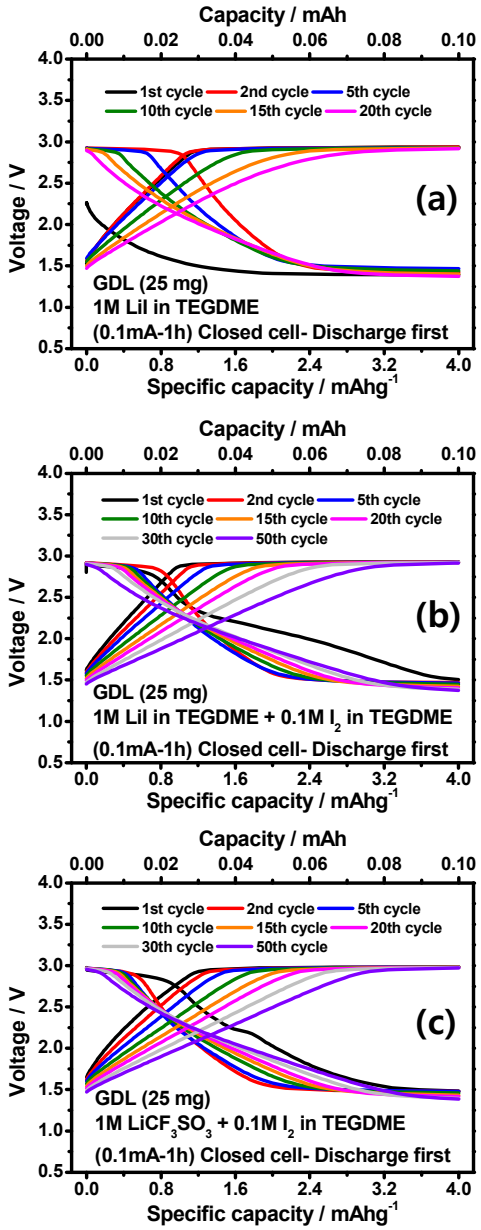

Figure 3. Galvanostatic cycling test response of same cells in Figure 2. without oxygen gas (closed cell): (a) 1 M LiI in TEGDME; (b) 1 M LiI + 0.1 M I_2 in TEGDME; and (c) 1 M $LiCF_3SO_3$ + 0.1 M I_2 in TEGDME at 0.1 mA current under time limit of 1 h.

Based on extensive previous work[26,27] and further confirmation obtained here as well, oxygen reduction produces Li_2O_2, together with some side reactions which precipitates on the electrodes.[28–33] The anodic curves reflect oxidation of the Li_2O_2 thus formed. As seen, the over-potentials for the anodic reaction (OER) increases with cycling and occurs above 4V .

When the ratio between the electrolyte solution volume and the cathode surface area is low enough, approaching what is relevant to practical batteries, as is the case of the coin type cells used herein, the cycle life of these systems is very limited. This is because of the inevitable side reactions that have already been studied[34,35], as well as the developing oxidative degradation of the carbon electrodes.[36,37]

Interestingly, there are differences between the voltage profiles of the first discharge process and subsequent ones. While the voltage profile of the first discharge is a flat plateau at around 2.7 V, subsequent discharge profiles show in the beginning shoulders at higher potentials (from 3.0-2.7 V) which converge to plateaus as discharge proceeds. We attribute these shoulders to reduction of unidentified side reaction products at potentials higher than that of oxygen reduction to Li-peroxide.

Electrochemical measurements of cells with high concentrations of LiI.

Figures 2a-c show the behavior of coin type cells in periodic galvanostatic cycling under oxygen atmosphere, where the TEGDME solutions contain high concentrations of LiI. Figures 2a and b describe cases where the solution is 1M LiI is the only electrolyte at 1 and 10 hours time limits, respectively. They show that in these cases the first discharge process is characterized by a plateau at around 2.75 V which reflects an irreversible process. At this stage, cycling proceeds very reversibly (hundreds cycles are possible). The second and subsequent reduction processes occur at potentials around 2.9-2.75 V, and the oxidation processes occur at potentials below 3.0 V. When 0.1 M I_2 is also present in solution (Figure 2c), there is no irreversible first discharge process. The first and subsequent discharge processes occur at the same potentials - in the range 2.9–2.75 V. Figure 2d shows the behavior of cells with 1M LiTF/TEGDME solution containing 0.1M I_2, with no initial LiI, in periodic galvanostatic cycling. The first discharge process is complicated, starting below 2.9

V and requires increasingly higher over-potentials, until reaching a plateau around 2.75 V. Then, subsequent cycling resembles the reversible behavior observed in Figure 2c (i.e., hundreds of cycles can be realized).

In order to properly understand the behavior of the cells presented in Figure 2, more experiments were necessary. Figures 3a-c present results of parallel experiments to those presented in Figures 2a-d (same cells and solutions), under argon atmosphere (i.e. hermetically sealed coin type cells). Three solutions were employed,, namely, TEGDME with 1M LiI, 1M LiI + 0.1M I_2, and LiTF + 0.1M I_2 (Figures 3a-c, respectively), and the cells exhibit reversible steady state cycling in the range 1.5– 3 V. The over-potentials of these processes are higher compared to the parallel processes under oxygen. In addition, these over-potential values decrease upon cycling. The first discharge processes in the three solutions, however, are different. In the presence of I_2, the first reduction process occurs at higher potentials compared to the subsequent discharge. On the other hand, without I_2, the first process occurs at lower potentials compared to the subsequent cycles (Figure 3a).

To complete our study, we explored the voltammetric and EQCM response of 0.01M LiI/TEGDME under oxygen (black line) and argon (red line) atmospheres (Figure 4), using 3 electrodes cells, where the working electrodes were platinum disks on thin quartz crystal sheets. Li foil served as the counter and reference electrodes. Low LiI concentration was used in order to obtain good resolution of the response at relatively high potential scanning rates, though the behavior observed should be relevant to higher LiI concentrations, as well. Figures 4a and b refer to the first and second cycles. The voltammetric response fully correlates, of course, to the galvanostatic response; however, it may provide a better overview of the entire electrochemical response of these systems.

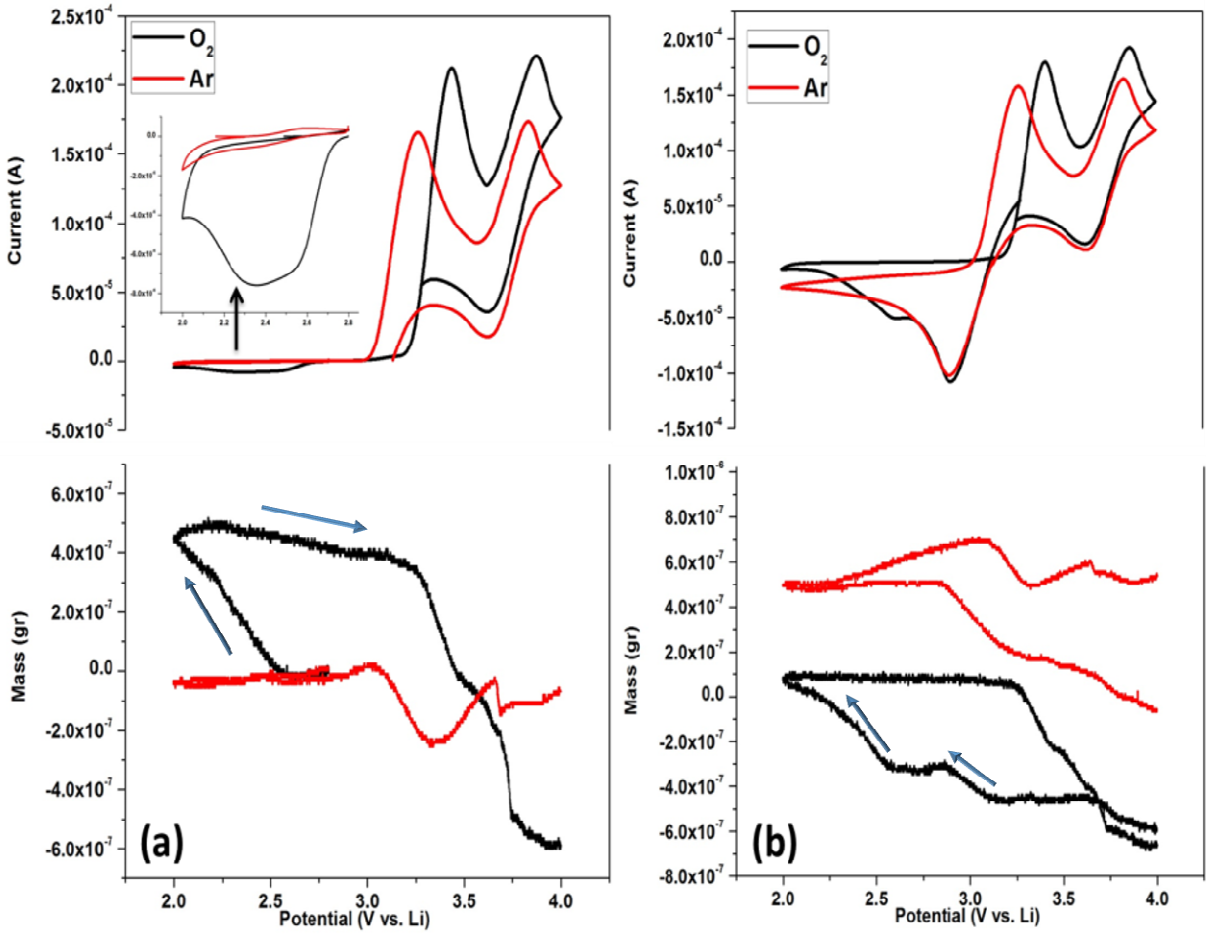

Figure 4. Cyclic voltammetry and EQCM response of platinum disks deposited on thin quartz crystals in 0.2 M LiTFSI + 0.01 M lithium iodide TEGDME at: (a) the 1st cycle; and (b) 2nd cycle, in oxygen (black lines) and argon (red lines) atmospheres.

Let us now focus on the red curves in Figure 4b which describe runs under argon , i.e., in the absence of oxygen. The typical red-ox behavior of iodine electrochemistry has been well characterized by previous studies of iodine electrochemistry in aqueous[38] and non-aqueous systems.[39] The two sets of peaks centering around 3.2 and 3.7 V vs. Li should be assigned to the I_3^-/I^- and I_2/I_3^- red-ox couples which undergo the equilibrium reactions

$I_3^- + 2e^- \rightleftharpoons 3I^-$ and $I_2 + I^- + e^- \rightleftharpoons I_3^-$, respectively. As seen in Figure 4a, since the solutions do not initially contain iodine, a first cathodic polarization shows no electrochemical process. In the first anodic polarization, iodine is formed and, hence, the

voltammogram shows the two expected oxidation peaks of the overall process $I^- \rightarrow I_3^- \rightarrow I_2$. In the second cycle (Figure 4b), the 2 sets of peaks of these red-ox processes are fully developed. In the presence of oxygen (black curves in Figure 4a and b), a first cathodic polarization show an irreversible process (see the broad shallow peak in the potential range of 2.75-2.0 V vs. Li in Fig. 4a).

Anodic polarization shows the two anodic peaks described above and further cycling of this system shows the two fully developed sets of peaks belonging to the two iodine related red-ox processes. In the presence of oxygen, the second (and subsequent) cyclic voltammogram of this system shows also a broad peak centered around 2.5 V, which appears as a shoulder to the cathodic peak centered around 2.8 V. The irreversible cathodic peak in the range 2.0-2.8 V seen in Figure 4, corresponds to the plateau around 2.7V seen in Figure 2a and should be assigned to oxygen reduction. The red-ox processes presented in Figures 2 and 3 (the cathodic and anodic voltage plateaus) relate to the first red-ox process around 3 V presented in Figure 4 (related to the I_3^-/I^- couple). The fact that only the first red-ox process appears in Figures 2 and 3 is because of the short time limits of 1 or 10 hours, that were set in the experiments.

The EQCM response of the electrodes under argon show some irreversible changes that were not explored. We speculate that they may relate to adsorption phenomena. The EQCM response of these cells under oxygen is interesting. The cathodic process in the first cycle is characterized by a pronounced mass increase, reflecting precipitation of insoluble reaction products. The subsequent anodic process is characterized by a mass decrease at potentials above 3.3V. The second cycle is also characterized by a mass increase during the cathodic scan and a subsequent mass decrease above 3.3V during the anodic scan. It is important to note the general similarity in the mass changes of the electrodes in the first and second cycles, despite the pronounced difference in the electrochemical response (see explanation below).

In order to complete our study of the electrochemical behavior of solutions with high LiI concentration, Figure 5 provides the typical chrono-potentiometric behavior (i.e. galvanostatic measurements) of the Li-C cells with 1M LiI/TEGDME solution under oxygen at different conditions than before. The time limitation of the experiment was extended to 20 hours and the first process was charging (oxidation), followed by cycling.

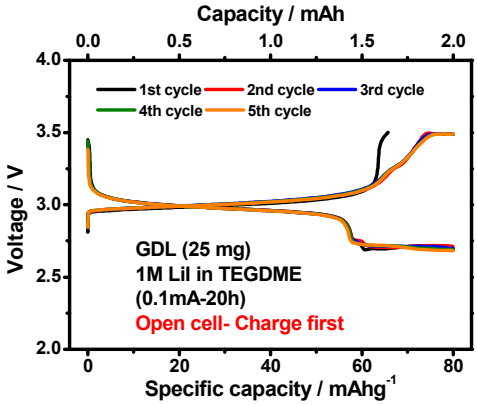

Figure 5. Galvanostatic charge first cycling test response of Li–O_2 cells using 1 M LiI in TEGDME electrolyte with higher capacity at 0.1 mA current under time limit of 20 h for checking further reaction and reaction order.

The data presented in this figure are fully parallel to the voltammetric response shown in Figure 4. A first oxidation process is observed as a plateau around 3 V (related to oxidation of I^- to I_3^-). An additional plateau emerges at around 3.5 V (we present here just the beginning of the process), which relates to the next red-ox couple of this system (oxidation of I_3^- to I_2). The cathodic processes shows the plateau ca. 2.9 V related to reduction of I_3^- to I^-, and then the low voltage plateau at around 2.5 V, which corresponds to the low potential, broad peak at the same voltage appearing in the voltammograms presented in Figure 4.

Understanding the electrochemical response of the Li-oxygen-LiI cells.

Several questions arise from the electrochemical behavior described in the previous section. Firstly, what is occuring in the cathodic reaction in the presence of oxygen with high concentration of LiI? The XRD of electrodes that underwent the cathodic process related to the plateau and peak appearing in Figures 2, 5 and 4 (respectively), showed only one product, namely, LiOH (see Figure 6). FTIR spectra of these electrodes (transmission mode with KBr pellets) clearly showed the sharp peak of hydrated LiOH at 3566-3573 cm^{-1}.[40] [The hydrated form is due to the ex-situ measurement and exposure to trace moisture.] LiOH was also the only product detected after the electrodes underwent a further cycling within the potential domain presented in Figure 4 and were taken out of the cells either after the cathodic process below 2.5 V or after the anodic process around 3.5 V. Hence, the mass changes recorded in the EQCM measurements under oxygen atmosphere (Figure 4) relate to the formation of LiOH in the cathodic processes (in first and subsequent cycles) and its decomposition at potentials above 3.3 V. It is quite possible that the use of platinum electrodes in the EQCM experiments enable the decomposition of LiOH at relatively low anodic potentials.

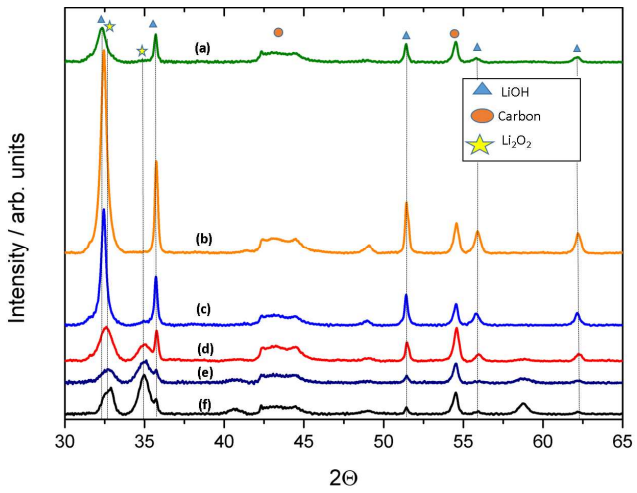

Figure 6. XRD patterns of GDL electrode discharged to 2 V using TEGDME with: (a) 1M LiI; (b) 1 M LiTFSI + 100 mM LiI; (c) 1 M LiTFSI + 10 mM LiI; (d) 1 M LiTFSI + 10 mM LiI stopped at 2.6 V; and (e) 1 M LiTFSI + 5 mM LiI (f) 1M LiTFSI.

LiOH was the main product detected on the cathodes (Figure 6) when the concentration of LiI (in 1M LiTF/TEGDME solutions) was reduced to 0.1M. However, when the concentration of LiI was reduced to 0.01M and even below that to 0.005M, the XRD patterns of electrodes after reduction showed the presence of both LiOH and Li_2O_2 (Figure 6). By comparison, Figure 6 presents XRD patterns of electrodes polarized cathodically in LiI free LiTF/TEGDME solutions, showing that Li_2O_2 is formed as the major oxygen reduction product. Note however, that some LiOH is formed even in the absence of LiI.

Several comments are in order at this junction. What we see in the galvanostatic charging response of the cells reflects reactions at lower over-potential, but we cannot assign it to LiOH oxidation. It is logical to assume that LiOH does not decompose at the potential window at which we work. Measurements of electrodes after the oxidation process showed that LiOH is still there. It is clear that the plateau we see in Figure 2 is the oxidation of the I^- and not OER. And this is another reason why iodide is not a good additive.

We would now like to comment on the fact that in comparing Figures 6a and 6b, we note that higher concentrations of LiI result in a relatively lower intensity. The conditions of each measurement (step size and the time at each step) were exactly the same for all electrodes. However, the intensities of the XRD peaks are not fully quantitative. These measurements show, from a qualitative perspective, the main products of the ORR. On a quantitative level, the intensities of the peaks depend on the position of the electrodes measured, which cannot be exactly the same for each measurement. Another important issue is that the substances measured were formed by electrochemical deposition, what makes them inherently different than powders (for which measurements can be indeed fully quantitative). Hence, we cannot say that there is a linear dependence of the LiI concentration and the amount of LiOH that was deposited. This issue, on its own, should be the subject of a follow-up study. It is also

important to note that differences in concentrations - 0.1M LiI vs. 1M LiI - may lead to a change in the morphology of the deposited LiOH. For instance, if the LiOH deposits are less crystalline at high LiI concentration, the intensity of the XRD patterns should be lower. Hence a simple comparison may not be justified.

Regarding the anode, we have previously shown[41] that polyethers are attacked by metallic lithium to form mostly lithium alkoxides. LiOH is formed on lithium due to the presence of trace moisture. LiOH when formed on the Li metal surface is supposed to be further reduced to Li_2O. Hence, the detection of LiOH on the cathodes is not connected to the Li anode side.

Figure 7 shows SEM images of a pristine electrode and electrodes polarized cathodically under oxygen atmosphere in LiI and LiTF solutions. The electrode treated in the LiI free solution show the well-recognized surface morphology of Li_2O_2 deposits, while the surface morphology of the electrode polarized in the LiI solution reflects the morphology of LiOH deposits, which differs pronouncedly from that of pristine and Li_2O_2 deposited electrodes.

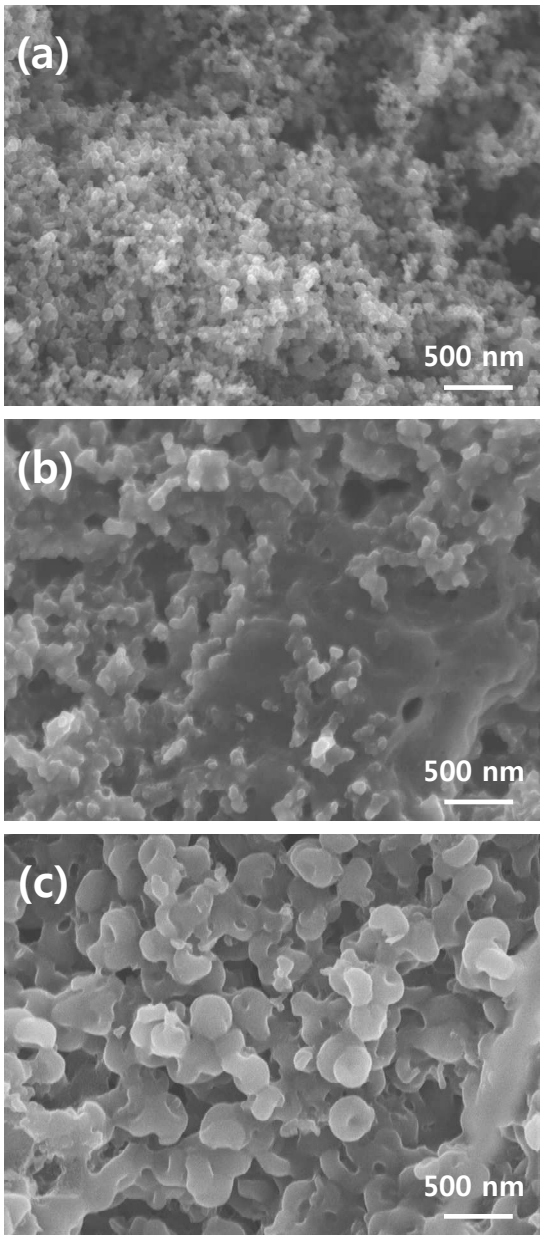

Figure 7. SEM images of oxygen electrode before and after 1st discharge: (a) Pristine GDL electrode; (b) GDL electrode discharged to 2 V using 1 M LiI in TEGDME electrolyte; and (c) GDL electrode discharged to 2 V using 1 M $LiCF_3SO_3$ in TEGDME electrolyte.

Since we could not detect Li_2O_2 species after oxygen reduction in the presence of iodine species, we examined the possibility that oxygen reduction occurs via the formation of superoxide moieties which interact with I_2 and or I_3^- (together with Li ions). The possible detection of, meta-stable Li-superoxide was examined by the Raman spectroscopy of cell

solutions containing LiI and I_2 that underwent oxygen reduction and *in-situ* EPR measurements during cycling. These species have Raman shifts[42] around 1100 cm^{-1} and characteristic EPR signals.[43]

Despite repeated efforts, we have not been able to detect any superoxide moieties in this system. These results do not rule out the formation of superoxide but merely indicate that superoxide does not exist in these systems as a detectable, meta-stable intermediate. The most logical explanation for the formation of LiOH as the major product of oxygen reduction in solutions containing high concentration of LiI is outlined in Scheme 2. Each step in this mechanism is well documented in our previous work and in the research of others, as delineated below.

(a)

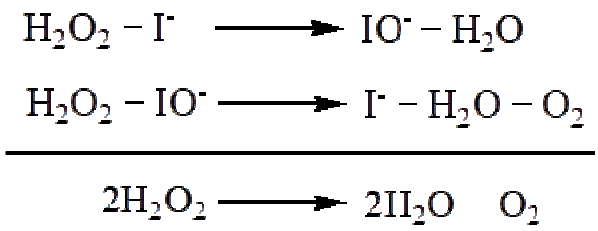

(b)

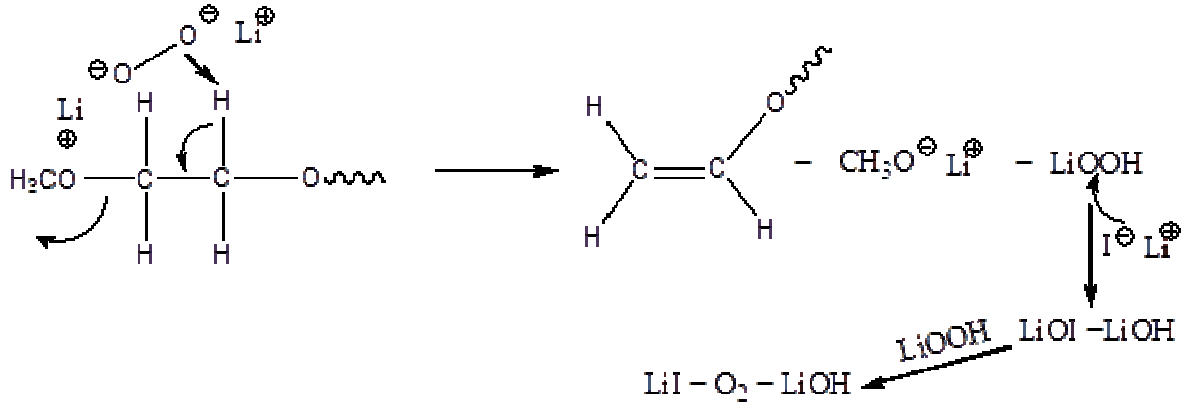

(c)

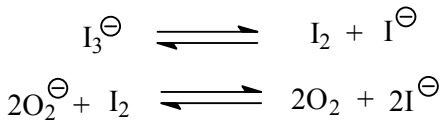

Scheme 2. (a) The decomposition reaction of hydrogen peroxide catalyzed by iodide.[44–46] (b) Proposed decomposition reaction mechanism of ether solvents in Li–O_2 cells containing LiI. (c) The proposed role of molecular oxygen as a red-ox mediator for a fast reduction of I_3^-, due to its reduction to super-oxide.[47,48]

Based on previous studies[44–46], it is known that iodide ion (I^-) catalyzes the decomposition of H_2O_2 to O_2 and H_2O (Scheme 2a), via the intermediate formation of IO^- , see scheme 2. We also know from our previous studies[34,49] that peroxy and superoxide anions are both strong bases and strong nucleophiles in aprotic ether solutions. As strong bases they can affect E2 elimination - with the ether group serving as the leaving group (see Scheme 2b). While alkoxides are generally poor leaving groups, such a process would be undoubtedly aided by the presence of the highly electrophilic Li ions which strongly complex with the non-bonding

electrons of the ether oxygens. Indeed, our previous studies in ether solutions clearly identified side products of oxygen reduction initiated by proton or hydrogen abstraction and yielded lithiated ionic compounds such as $LiOCH_3$.[34] Based on this work, we suggest that the most logical pathway of LiOH formation - formed exclusively at high concentration of LiI in the ether solutions – involves the following steps (Scheme 2b). Firstly, lithium peroxide or superoxide formed by oxygen reduction in the electrolysis effect E2 elimination which results in the generation of LiOOH. The presence of LiI drives the fast decomposition of LiOOH to LiOH and LiOI. The latter reacts in turn with additional LiOOH leading to the generation O_2, LiI and more LiOH, as outlined in Scheme 2b.

The results of this study demonstrate clearly the importance of side reactions in Li-oxygen cells, due to the nucleophilic and basic nature of the superoxide and peroxide species formed by oxygen reduction. Once these species are formed, there is competition between two processes. One is the columbic interactions of these oxygen species with Li ions that leads to the precipitation of Li_2O_2, which is not too reactive in the solid state. The second is the interaction of peroxide and superoxide with solvent molecules (assisted by the electrophilic Li counterions in solutions), which lead to side reactions. The presence of I^- pushes this delicate balance towards the side reactions, as outlined above. In the presence of LiI at high concentration, oxidation leads to the formation of I_3^-. Hence, if the capacity is limited and passivation does not occur – as is the case here - the red-ox reactions of the I_3^-/I^- which occur at higher potentials that those of oxygen reduction, dominate the electrochemical response of these cells, as presented in the Figure 2.

Another highly interesting question relates to the remarkable difference in the response of these systems, with and without oxygen - although in both cases, we are in fact measuring the electrochemical response of the I_3^-/I^- couple, generated in these cells. It appears that at high concentration of LiI, the presence of oxygen facilitates and promotes the reduction of I_3^-. We

can explain this red-ox mediation of oxygen in these cells based on previous work that explored reactions of superoxide species and halogen compounds[47,48] , as outlined in Scheme 2c. As is well known, I_3^- is in equilibrium with I_2 and I^-. Superoxide moieties which are formed as very short-lived intermediates by oxygen reduction at relatively high potentials (close to 3 V)[42,50], easily transfer electrons to I_2 species, which yields I^- and molecular oxygen.

On the possible role of iodine species as red-ox mediators for oxygen electrochemistry.

Figure 8(a-d) shows the electrochemical response of cells containing different concentrations of LiI in LiTF/TEGDME solutions under oxygen atmosphere. The first reduction process occurs at low potentials in the range 2.75-2.5 V, as discussed above. As the concentration of LiI is lowered (in the milimolar level), Li_2O_2 becomes the dominant reduction product (Figure 6).

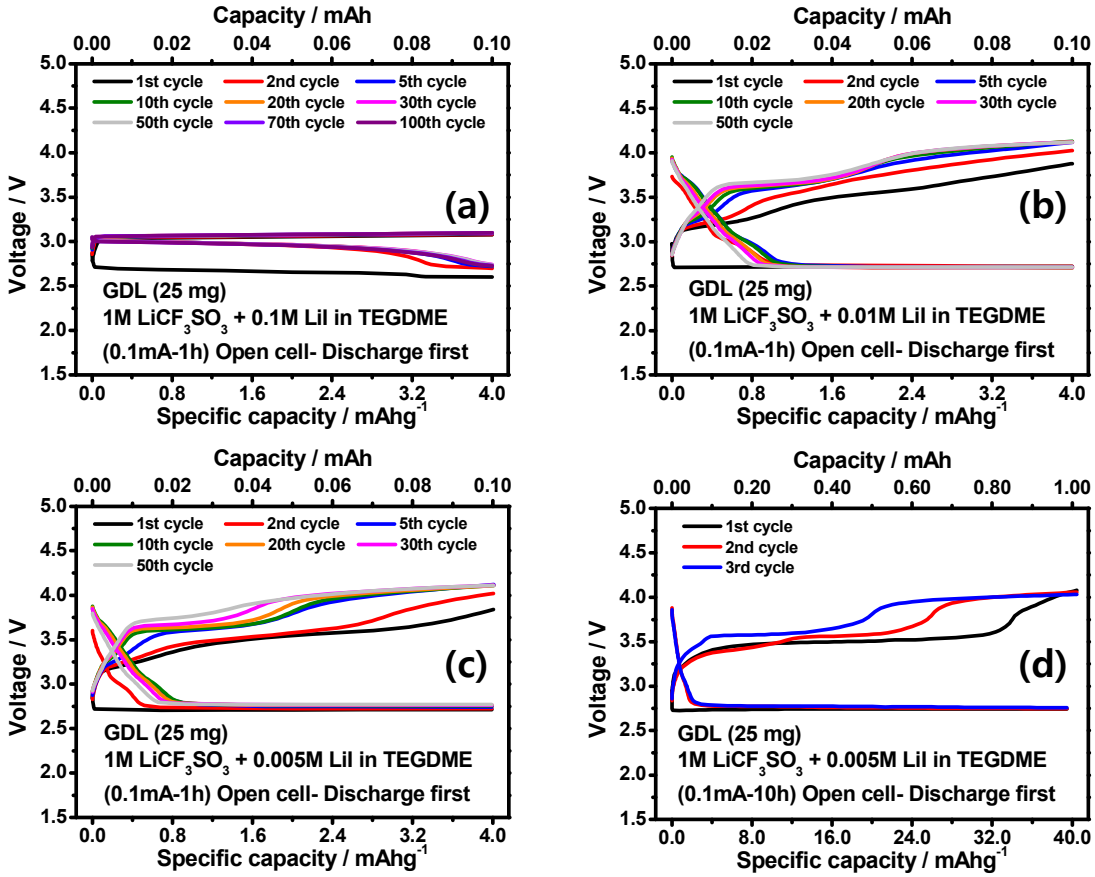

Figure 8. Galvanostatic cycling test response of Li–O_2 cells: (a) 1 M $LiCF_3SO_3$ + 0.1 M LiI in TEGDME; (b) 1 M $LiCF_3SO_3$ + 0.01 M LiI in TEGDME; (c) 1 M $LiCF_3SO_3$ + 0.005 M LiI in TEGDME at 0.1 mA current under time limit of 1 h; (d) 1 M $LiCF_3SO_3$ + 0.005 M LiI in TEGDME under time limit of 10 h.

Upon cycling, subsequent reduction processes are characterized (in galvanostatic measurements) by a short plateau, which becomes shorter as the concentration of LiI is lowered, and the low potential plateau that reflects formation of Li_2O_2 becomes longer. Hence, as the concentration of I^- drops, it affects less and less the competing side reaction that forms LiOH. Once Li_2O_2 is the major oxygen reduction product, I_2 which is obviously formed during oxidation, can react as red-ox mediator for an easy oxidation of the solid Li peroxide thus formed. This is reflected by the lower potentials required for the anodic process: below 4 V, as seen in Figure 8d. This should be compared to >4.3V required to oxidized solid Li_2O_2 precipitated on carbon electrodes in ether solutions (without electrocatalysis), as clearly seen in Figure 1b. This behavior is clearly seen in the Figure 8 and has also been reported by others.[50]

Conclusions.

This work has focused on the electrochemistry of Li-oxygen systems, on carbon and platinum electrodes using glyme polyether solutions (primarily TEGDME) with various concentrations of LiI. The motivation for this study came from an earlier reports on the use of LiI as a superb red-ox mediator in I-oxygen cells, which facilitates the oxidation of Li-peroxide at low over-potentials. The present work showed that LiI at high concentrations in ethereal solutions, promotes side reactions, in which the oxygen anionic species (superoxide and peroxide) formed by oxygen reduction, attack solvent molecules, leading to precipitation on the electrodes surface of LiOH as the major product rather than Li_2O_2. All such side reactions in

which solvent molecules are involved, results in solvent decomposition. The concomitant formation of LiOH rather than Li_2O_2 reduces the capacity of the Li-oxygen battery and is a major drawback in the use of LiI as a redox additive. Iodide ion (I^-) encourages the side reactions which involve proton abstraction by reacting quickly with the LiOOH species thus obtained, to form LiOH and LiOI. The latter reacts further with LiOOH leading to molecular oxygen, LiOH and LiI. These suggestions are based on previous conclusive studies that have illuminated the main steps of the mechanism proposed herein. We see, then, that when dealing with oxygen electrochemistry in non-aqueous systems in the presence of Li ions, catalysis can enhance side reactions.

Another interesting finding of this work relates to the fact that at high LiI concentrations in these Li-oxygen cells, the electrochemistry of the I_3^-/I^- and I_2/I_3^- couples dominates the cells' response. The presence of oxygen was found to serve as a red-ox mediator that facilitates I_3^- reduction. Based on a previous work, it is likely that this process involves superoxide formation followed by fast electron transfer to iodine. At low concentrations of LiI, the side reaction that forms LiOH is negligible and the main oxygen reduction product is Li_2O_2. Under these conditions, the I_2 formed by I^- oxidation can serve as a red-ox mediator for Li-peroxide oxidation. This study further demonstrates the importance of side reactions in Li-oxygen cells as one of their main limiting factors.

Acknowledgement.

This work at Hanyang University was supported by the Human Resources Development program (No. 20124010203310) of the Korea Institute of Energy Technology Evaluation and Planning (KETEP) grant funded by the Korea government Ministry of Trade, Industry and Energy and also supported by the Global Frontier R&D Program (2013M3A6B1078875) on Center for Hybrid Interface Materials (HIM) funded by the Ministry of Science, ICT &

Future Planning. Partial support for this work was obtained from the ISF, Israel Science Foundation, in the framework of the INREP project. A.A.F. thanks the Israel Science Foundation (Grant No. 1469/13) as well as the Ethel and David Resnick Chair in Active Oxygen Chemistry for their kind and generous support.

References.

1. K. Abraham and Z. Jiang, *J. Electrochem. Soc.*, 1996, **143**, 1–5.

2. J. Read, *J. Electrochem. Soc.*, 2002, **149**, A1190–A1195.

3. J. Read, K. Mutolo, M. Ervin, W. Behl, J. Wolfenstine, A. Driedger, and D. Foster, *J. Electrochem. Soc.*, 2003, **150**, A1351–A1356.

4. S. S. Sandhu, J. P. Fellner, and G. W. Brutchen, *J. Power Sources*, 2007, **164**, 365–371.

5. R. E. Williford and J.-G. Zhang, *J. Power Sources*, 2009, **194**, 1164–1170.

6. J. Xiao, D. Wang, W. Xu, D. Wang, R. E. Williford, J. Liu, and J.-G. Zhang, *J. Electrochem. Soc.*, 2010, **157**, A487.

7. X. Yang and Y. Xia, *J. Solid State Electrochem.*, 2009, **14**, 109–114.

8. A. Debart, J. Bao, G. Armstrong, and P. G. Bruce, in *ECS Transactions*, ECS, 2007, vol. 3, pp. 225–232.

9. Y.-C. Lu, H. A. Gasteiger, M. C. Parent, V. Chiloyan, and Y. Shao-Horn, *Electrochem. Solid-State Lett.*, 2010, **13**, A69.

10. Y.-C. Lu, E. J. Crumlin, G. M. Veith, J. R. Harding, E. Mutoro, L. Baggetto, N. J. Dudney, Z. Liu, and Y. Shao-Horn, *Sci. Rep.*, 2012, **2**, 715.

11. R. Wen, M. Hong, and H. R. Byon, *J. Am. Chem. Soc.*, 2013, **135**, 10870–6.

12. S. E. Herrera, A. Y. Tesio, R. Clarenc, and E. J. Calvo, *Phys. Chem. Chem. Phys.*, 2014, **16**, 9925–9.

13. Z. Peng, S. A. Freunberger, Y. Chen, and P. G. Bruce, *Science*, 2012, **337**, 563–6.

14. N. Mozhzhukhina, L. P. Méndez De Leo, and E. J. Calvo, *J. Phys. Chem. C*, 2013, **117**, 18375–18380.

15. N. Tsiouvaras, S. Meini, I. Buchberger, and H. a. Gasteiger, *J. Electrochem. Soc.*, 2013, **160**, A471–A477.

16. B. D. McCloskey, R. Scheffler, A. Speidel, D. S. Bethune, R. M. Shelby, and a C. Luntz, *J. Am. Chem. Soc.*, 2011, **133**, 18038–41.

17. A. A. Frimer, in *Superoxide Dismutase*, ed. Oberley L.W, Chemical Rubber Company, Boca Raton, Florida, 1982, pp. 83–125.

18. A. A. Frimer, in *The Chemistry of Peroxides*, ed. S. Patai, Wiley, London, 1983, pp. 429–461.

19. B. D. McCloskey, R. Scheffler, A. Speidel, D. S. Bethune, R. M. Shelby, and A. C. Luntz, *J. Am. Chem. Soc.*, 2011, **133**, 18038–18041.

20. S. A. Freunberger, Y. Chen, N. E. Drewett, L. J. Hardwick, F. Bardé, and P. G. Bruce, *Angew. Chem. Int. Ed. Engl.*, 2011, **50**, 8609–8613.

21. D. Sharon, V. Etacheri, A. Garsuch, M. Afri, A. A. Frimer, and D. Aurbach, *J. Phys. Chem. Lett.*, 2013, **4**, 127–131.

22. C. O. Laoire, S. Mukerjee, K. M. Abraham, E. J. Plichta, and M. A. Hendrickson, *J. Phys. Chem. C*, 2009, **113**, 20127–20134.

23. S. Meini, N. Tsiouvaras, K. U. Schwenke, M. Piana, H. Beyer, L. Lange, and H. A. Gasteiger, *Phys. Chem. Chem. Phys.*, 2013, **15**, 11478–11493.

24. H.-D. Lim, H. Song, J. Kim, H. Gwon, Y. Bae, K.-Y. Park, J. Hong, H. Kim, T. Kim, Y. H. Kim, X. Lepró, R. Ovalle-Robles, R. H. Baughman, and K. Kang, *Angew. Chem. Int. Ed. Engl.*, 2014, **53**, 3926–3931.

25. K. J. Hanson, *J. Electrochem. Soc.*, 1987, **134**, 2204.

26. M. M. Ottakam Thotiyl, S. a Freunberger, Z. Peng, Y. Chen, Z. Liu, and P. G. Bruce, *Nat. Mater.*, 2013, **12**, 1050–6.

27. H.-G. Jung, J. Hassoun, J.-B. Park, Y.-K. Sun, and B. Scrosati, *Nat. Chem.*, 2012, **4**, 579–85.

28. D. G. Kwabi, T. P. Batcho, C. V. Amanchukwu, N. Ortiz-Vitoriano, P. Hammond, C. V. Thompson, and Y. Shao-Horn, *J. Phys. Chem. Lett.*, 2014, **5**, 2850–2856.

29. K. U. Schwenke, S. Meini, X. Wu, H. a Gasteiger, and M. Piana, *Phys. Chem. Chem. Phys.*, 2013, **15**, 11830–9.

30. Y. Chen, S. a Freunberger, Z. Peng, F. Bardé, and P. G. Bruce, *J. Am. Chem. Soc.*, 2012, **134**, 7952–7.

31. M. J. Trahan, S. Mukerjee, E. J. Plichta, M. A. Hendrickson, and K. M. Abraham, *J. Electrochem. Soc.*, 2012, **160**, A259–A267.

32. S. a Freunberger, Y. Chen, Z. Peng, J. M. Griffin, L. J. Hardwick, F. Bardé, P. Novák, and P. G. Bruce, *J. Am. Chem. Soc.*, 2011, **133**, 8040–7.

33. S. a Freunberger, Y. Chen, N. E. Drewett, L. J. Hardwick, F. Bardé, and P. G. Bruce, *Angew. Chem. Int. Ed. Engl.*, 2011, **50**, 8609–13.

34. D. Sharon, V. Etacheri, A. Garsuch, M. Afri, A. A. Frimer, and D. Aurbach, *J. Phys. Chem. Lett.*, 2013, **4**, 127–131.

35. D. Sharon, D. Hirsberg, M. Afri, A. Garsuch, A. a. Frimer, and D. Aurbach, *J. Phys. Chem. C*, 2014, **118**, 15207–15213.

36. B. D. McCloskey, A. Speidel, R. Scheffler, D. C. Miller, V. Viswanathan, J. S. Hummelshøj, J. K. Nørskov, and A. C. Luntz, *J. Phys. Chem. Lett.*, 2012, **3**, 997–1001.

37. M. M. Ottakam Thotiyl, S. a. Freunberger, Z. Peng, and P. G. Bruce, *J. Am. Chem. Soc.*, 2013, **135**, 494–500.

38. Y. Zhao, L. Wang, and H. R. Byon, *Nat. Commun.*, 2013, **4**, 1896.

39. K. J. Hanson and C. W. Tobias, 1987, **115**, 2204–2210.

40. E. C. S. Transactions and T. E. Society, 2010, **33**, 223–229.

41. D. Aurbach, E. Granot, and R. Gan, *Electrochim. Acta*, 1997, **42**, 697–718.

42. L. Johnson, C. Li, Z. Liu, Y. Chen, S. a. Freunberger, J.-M. Tarascon, P. C. Ashok, B. B. Praveen, K. Dholakia, and P. G. Bruce, *Nat. Chem.*, 2014, **6**, 1091–1099.

43. P. Pieta, A. Petr, W. Kutner, and L. Dunsch, *Electrochim. Acta*, 2008, **53**, 3412–3415.

44. H. A. Liebhafsky, *J. Am. Chem. Soc.*, 1932, **54**, 3499–3508.

45. H. A. Liebhafsky, *J. Am. Chem. Soc.*, 1932, **54**, 1792–1806.

46. H. A. Liebhafsky, *J. Am. Chem. Soc.*, 1934, **56**, 2369–2372.

47. H. A. Schwarz and B. H. J. Bielski, *J. Phys. Chem.*, 1986, **90**, 1445–1448.

48. S. Kim, R. DiCosimo, and J. San Filippo, *Anal. Chem.*, 1979, **51**, 679–681.

49. D. Sharon, M. Afri, M. Noked, A. Garsuch, A. A. Frimer, and D. Aurbach, *J. Phys. Chem. Lett.*, 2013, **4**, 3115–3119.

50. C. O. Laoire, S. Mukerjee, K. M. Abraham, E. J. Plichta, and M. A. Hendrickson, *J. Phys. Chem. C*, 2010, **114**, 9178–9186.